

Analysis of volunteer observing ship temperature fields in the tropical Atlantic Ocean

Temperature fields
Tropical Atlantic Ocean
Volunteer observing ships
SEQUAL/FOCAL experiment

Champs de température
Océan Atlantique tropical
Navires d'observation volontaires
Expérience SEQUAL/FOCAL

Dennis A. MAYER^a, Robert L. MOLINARI^a, Robert H. WEISBERG^b

^a Atlantic Oceanographic and Meteorological laboratory, National Oceanic and Atmospheric Administration (NOAA), 4301 Rickenbacker Causeway, Miami, Florida 33149, USA.

^b Department of Marine Science, University of South Florida, 140, 7th avenue, South, St. Petersburg, Florida 33701, USA.

Received 3/10/89, in revised form, 3/1/90, accepted 11/1/90.

ABSTRACT

Volunteer observing ship data collected during the FGGE year in 1979 and data from *in situ* moorings deployed during the SEQUAL/FOCAL experiment in 1983-1984 are used to estimate the dominant temporal and spatial scales of SST variability in the equatorial Atlantic Ocean. Two-dimensional Fourier transforms show that enhanced energy levels in a wave number and frequency band of 1924^{-1} - 825^{-1} cycles/km and 37^{-1} - 21^{-1} cycles/day respectively, are associated with organized SST structures with wave-like oscillations that are consistent with barotropic instabilities. The oscillations appear on the equator between 1°S and 1°N eastward of 25°W shortly after the springtime intensification of the easterly wind stress and persist into August. They are characterized by a westward phase propagation of about -50 cm/s and a pattern that progresses eastward at approximately 30 cm/s.

Oceanologica Acta, 1990, 13, 3, 257-264.

RÉSUMÉ

Champs de température relevés par les navires d'observation volontaires dans l'Océan Atlantique tropical

Les principales échelles temporelles et spatiales de variabilité de la température superficielle dans l'Atlantique équatorial sont estimées à partir des données obtenues en 1979 par les navires d'observation volontaires pendant l'expérience FGGE et à partir des données acquises par les bouées ancrées déployées pendant l'expérience SEQUAL/FOCAL en 1983-1984.

Les transformées bidimensionnelles de Fourier montrent que des niveaux d'énergie renforcés dans une gamme de 1924^{-1} à 825^{-1} cycles/km en nombre d'ondes et 37^{-1} à 21^{-1} cycles/jour en fréquence, sont associés à des structures organisées de températures superficielles où des oscillations sont compatibles avec des instabilités barotropes. Les oscillations apparaissent à l'équateur entre 1°S et 1°N , à l'est du méridien 25°W , peu après l'intensification printanière de la tension du vent d'Est. Elles durent jusqu'au mois d'août; elles sont caractérisées par une vitesse de phase vers l'Ouest d'environ 50 cm/s et une vitesse de groupe vers l'Est d'environ 30 cm/s.

Oceanologica Acta, 1990, 13, 3, 257-264.

INTRODUCTION

The exchange of energy across the air-sea interface in the tropical oceans has been recognized as a major factor in determining both regional and global atmospheric climate variability. The intensity of this exchange is a function of sea surface temperature (SST). Because of this dependence, the study of SST in the

tropics represents a major focus of the Tropical Ocean Global Atmosphere (TOGA) Program. TOGA is an internationally coordinated effort directed at defining the effects of the tropical oceans on global climate. A specific objective of TOGA is to obtain a data-set defining upper ocean conditions, including SST over a ten-year period. This data-set will be used in dynamical studies, numerical model verification efforts, and as input for prognostic model runs.

Merchant volunteer observing ships (VOS) can provide an important source of both historical and recent SST data for TOGA and other studies. Herein, an attempt has been made to develop an analysis tool for use on VOS data and to use this tool to delineate the dominant temporal and spatial scales in one-year long records of SST fields. The fields were obtained from VOS during the first GARP Global Experiment (FGGE) conducted in the tropical Atlantic Ocean in 1979.

These data are analyzed in the frequency and zonal wave number domains in an attempt to define bands over which the variance may be described by organized structures. Wherever possible, the evolving fields of SST will be considered in terms of what is presently understood about upper ocean thermal and velocity variability on the equator. For these purposes, the

discussion of instability waves in the equatorial Atlantic Ocean by Weisberg and Weingartner (1988) is relevant since the SST signatures of these waves are manifest in the VOS data.

DATA

The FGGE year extended from December 1978 through November 1979. The VOS coverage typically available for the central equatorial Atlantic was augmented during FGGE by research vessel observations. A complete set of monthly SST maps is given in Molinari *et al.* (1985). Representative SST distributions and data coverage are given in Figure 1. Locations of the

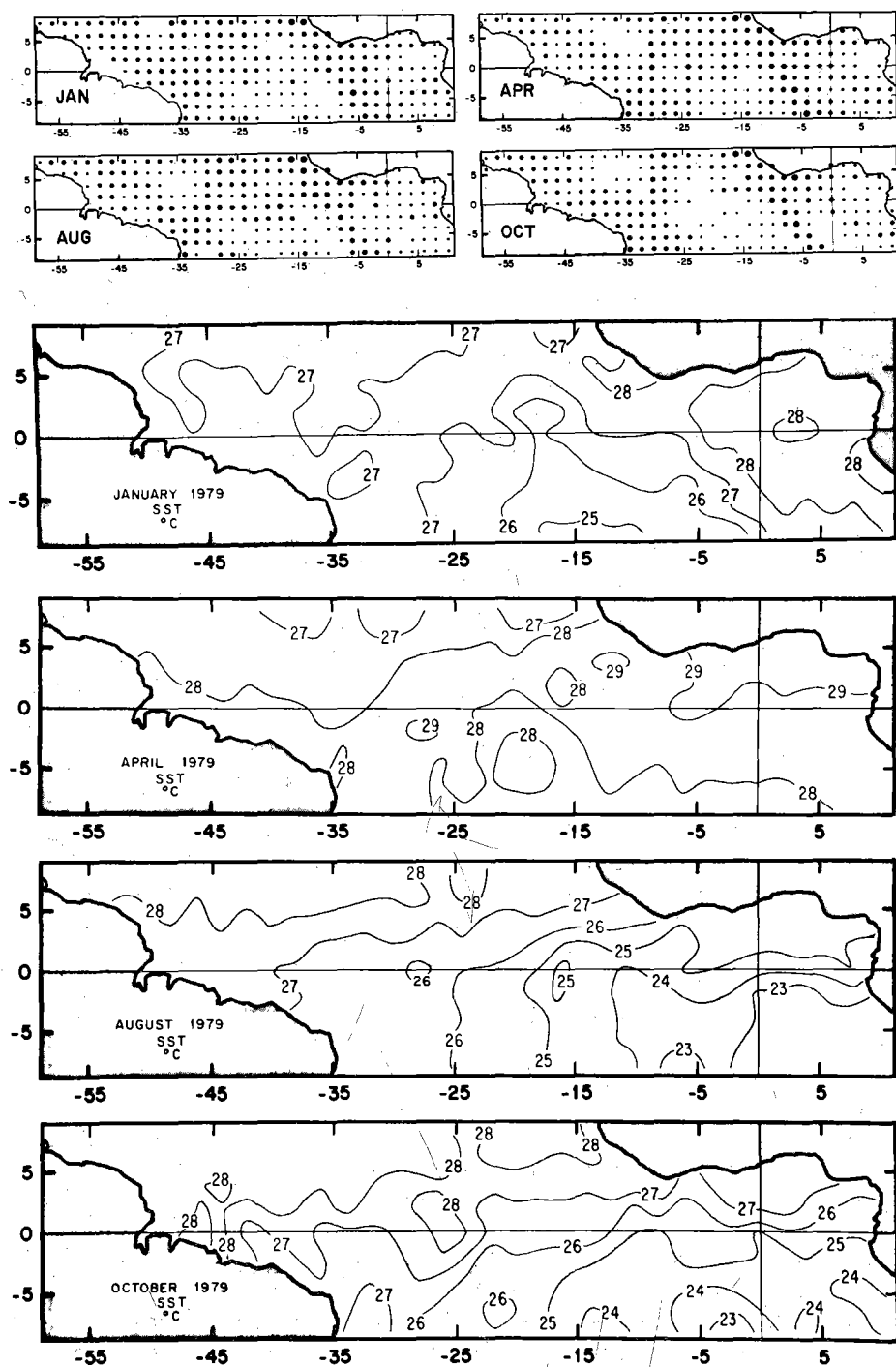


Figure 1
 Monthly distribution of surface observations for January, April, August and October 1979, on a 2x2 grid. Dot size corresponds to number of observations in the month: smallest dot stands for 1-4 observations; next larger, 5-14 observations; next larger, 15-24 observations; largest, 25-31 observations.

main shipping lanes are obvious. In earlier studies using these data, Molinari *et al.* (1985) averaged the VOS data by 2° quadrangles and month and described the evolution of the large-scale SST fields. Briefly, a large annual signal in tropical SST is characterized by intense cooling in the late spring-summer time frame (Fig. 1). By mid- to late summer, close to the equator, a large pool of cold water is found centered upon approximately 10°W in the Gulf of Guinea. Normally the lowest SST's are observed at this time and are associated with intense horizontal SST gradients. Basin-wide warming and the disappearance of the cold water pool occurs in the fall. Highest SST's occur near the end of winter and are associated with the smallest horizontal SST gradients. Molinari *et al.* (1985) show that on a monthly time scale, FGGE year SST time series are in phase with the climatological time series of Reynolds (1985).

Herein, spatial resolution is also only 2°, or about 222 km on the equator. Temporal resolution is increased to one week. The demeaned FGGE SST field between 1°S and 1°N extending from 3°E to 49°W is contoured in Figure 2. Data-void areas which represent

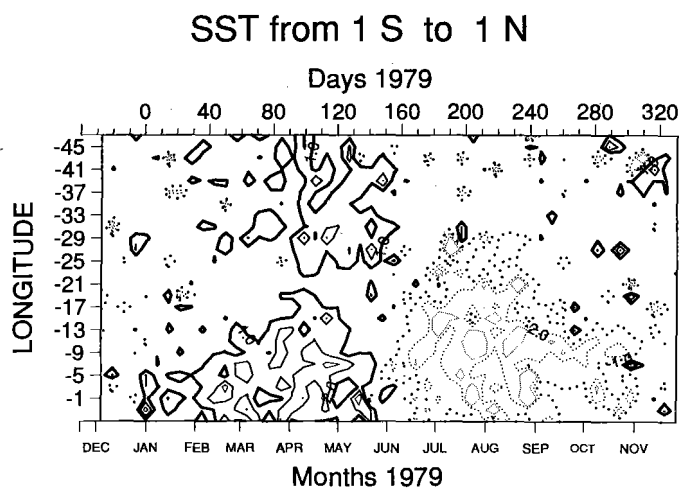


Figure 2
Demeaned SST observations on the equator for FGGE year December 1978 through November 1979. Contour interval is 1.0 with 0°C contour suppressed. Dashed and solid contours denote negative and positive values respectively.

about 29% of the areal coverage on the equator were filled with the lowest frequency and wave number SST fields (described below). Although other zonal bands north and south of the equator were analyzed as well, most of the energy that was organized and that could be compared with other data sets (described below) was observed in the 1°S to 1°N band.

Temperature data were also collected during the 1983-1984 SEQUAL/FOCAL (S/F) experiments. A portion of these data were obtained from sensors placed on equatorial current meter moorings near the longitudes 28°, 24°, 15° and 4°W (Weisberg and Weingartner, 1988). The data from a depth of 10 m are essentially equivalent to SST (Weisberg and Weingartner, 1988) and can therefore be compared to the FGGE VOS data. Although the S/F spatial coverage is somewhat limited, the 1-hour temporal resolution is much better than the weekly VOS data. Realistically, to compare

with the weekly VOS data, the S/F data were 13-day, low-pass (LP) filtered (6 db down at 13 days and 20 db down at 10 days) and are plotted in Figure 3. The VOS data are also plotted in Figure 3 for the four available longitudes (28°, 24°, 14° and 4°W) that are comparable to the S/F longitudes.

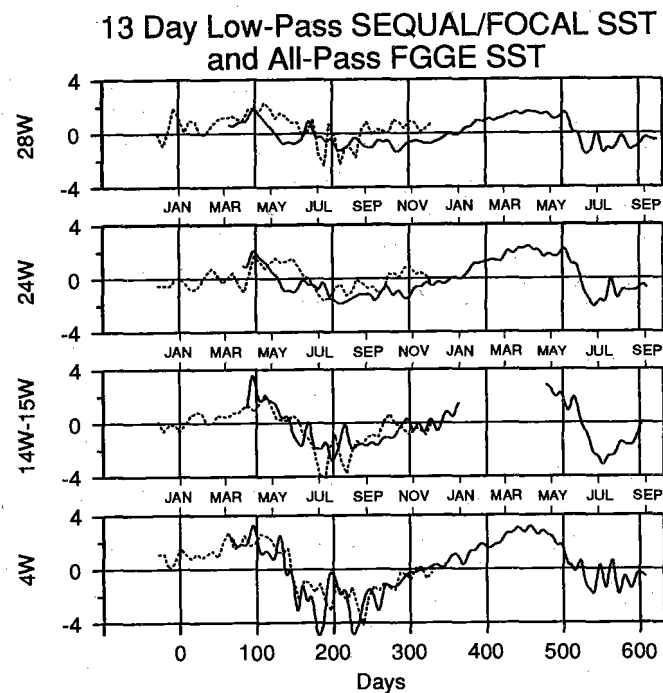


Figure 3
Thirteen-day, LP filtered S/F SST data from 1983-1984, and FGGE-VOS demeaned SST time series from 1979. Zero days indicates January of 1979/1983. Longitudes correspond to S/F longitudes except for 15°W where 14°W is plotted for FGGE data.

ANALYSIS

Two-dimensional Fourier transforms are utilized to examine the evolving zonal temperature fields. Regions of higher energy (variance) can be identified from a contour plot of the two-dimensional transform (fractional variance as a function of wave number and frequency, *see* the Appendix). Further, by inverting a particular band, the temporal and spatial structure of this band can be described by plotting the inverted field. We have defined an all-pass (AP) filtered band (discussed below) from $m=0-10$ harmonics in space and from $n=0-18$ harmonics in time. The two-dimensional transform of this field is contoured in Figure 4. The fundamental wavelength in space is 26-2° intervals which corresponds to a wave number of about 5772^{-1} cycles/km. In time, the fundamental period is 365 days. Because the sample intervals of the space and time grid are 2° (222 km) and 1 week respectively, some aliasing of the energy distribution in Figure 4 is manifest in the higher wave numbers above the 10th space harmonic (wave numbers near 577^{-1} cycles/km) and in the higher frequencies above the 18th time harmonic (frequencies near 20^{-1} cycles/day). These bands are therefore not included in the analysis (hence the limits of the AP band). Energy that would

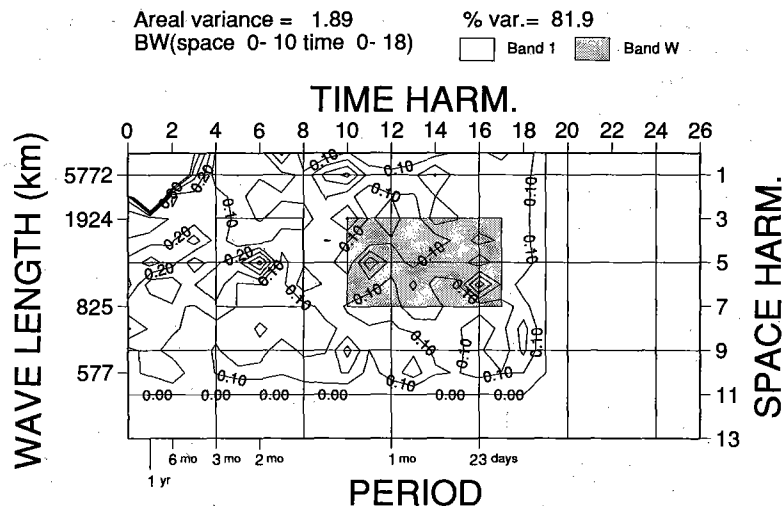


Figure 4
 Fractional variance as a function of wave number and frequency up to AP limits of $m=0-10$ (wave numbers to 577^{-1} cycles/km) and $n=0-18$ (frequencies to 20^{-1} cycles/day). Fractional variance is in terms of AP variance ($1.55^{\circ}C^2$, Tab. 1). Band 1 and band W indicated.

have been aliased apply to wavelengths less than about 500 km and periods less than about 19 days ($m > 10$, and $n > 18$ respectively). Similar to the 2° of freedom (dof) one-dimensional periodogram, the number of dof for each harmonic is 4 because each (m, n) amplitude estimate is computed with 4 coefficients (see Appendix). Figure 4 is simply a frequency and wave number periodogram for the VOS data within the equatorial region.

By setting the space and time harmonics $m > 3$ (wave-number greater than 1924^{-1} cycles/km) and $n > 4$ (frequencies greater than 91^{-1} cycles/day) respectively equal to zero and then inverting the two-dimensional transform, a LP filtered data set is arrived at as shown in Figure 5. Maximum energy is organized across the sequence of space harmonics centered on the annual period ($n = 1$). The maximum value is at the zero space harmonic ($m = 0$) and, for $m > 0$, the fractional variance is roughly proportional to $(1/m)^2$. Generally, any variance organized along the $m = 0, n \neq 0$ or $m \neq 0$ and $n = 0$ simply reflects a two-dimensional structure that cannot be resolved by the available data. The $m = 0, n = 0$ coefficient of course is just the areal mean. As described above, the missing data in the VOS SST field were filled (edited and filled SST field in Figure 2) with the LP filtered field in Figure 5.

In Table 1, the energy distribution is given for the demeaned SST field (Fig. 2) and the AP and LP filtered bands. In Table 2, the energy distribution as a fraction of the total field variance as represented by the AP filtered SST field is summarized for the largest energy peaks described by the contours in Figure 4. Two

Table 1
 Energy distribution. Variances for the demeaned SST field and the AP and LP fields ($^{\circ}C^2$).

	SST variance	Percent of SST variance
Demeaned SST	1.89	100
AP	1.55	82
LP	1.08	57

Low-pass SST from 1 S to 1 N

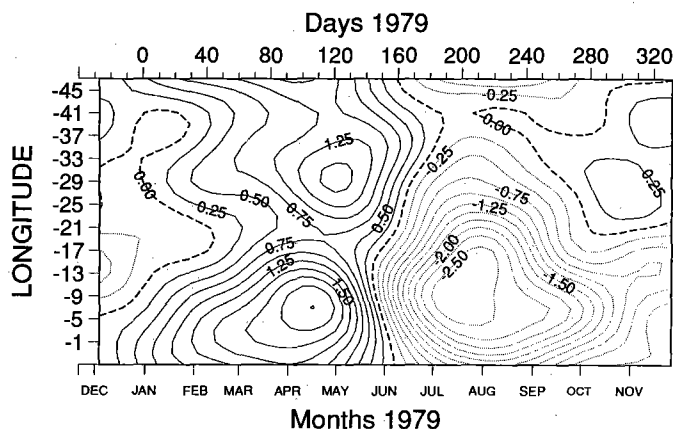


Figure 5
 LP demeaned SST observations for $m=0-3$ (wave numbers to 1924^{-1} cycles/km) and $n=0-4$ (frequencies to 91^{-1} cycles/day). Contour interval is $0.25^{\circ}C$. Dashed and solid contours denote negative and positive values respectively.

bands of increased variance are identified (band 1 and band W) and further analyzed.

The LP filtered fields in Figures 3 and 5 are consistent with the description of the SST fields given earlier. The highest temperatures are centered near JD 100-110 (April) and the minimum SST's are centered near JD 200-210 (end of July). Thus, there is some asymmetry in the annual signal, with only about 100 days separating the peak and trough. Both the demeaned field (Fig. 2) and the LP filtered field (Fig. 5) exhibit a maximum annual range in the SST signal of about $\pm 3^{\circ}C$ in the eastern basin. Comparison of the two seasons in SST for 1978 and 1983 in Figure 3 shows remarkable similarity except for some spikiness in the FGGE data (possibly caused by some aliasing in the analysis of the weekly VOS data). As noted in Weisberg and Colin (1986), not only does the Gulf of Guinea have the coldest SST along the equator in the Atlantic Ocean during summer, it also has the warmest SST during winter/spring.

Similar contour plots in time and space (as described for Figure 5 above) may be computed by inverting the two-dimensional transform (periodogram) over specified frequency and wave number bands. The number of dof for each band is $4 \times (\# \text{ of space harmonics}) \times (\# \text{ of time harmonics})$. The two bands denoted by band 1 (100 dof) and band W (160 dof) are shown in Figures 6 and 7, respectively. Phase propagation for the organized SST structures can be inferred by noting the slope of isotherms. For eastward propagation, one moves eastward along the isotherm in the direction of increasing time, and conversely for westward propagation.

Common to both bands is a noticeable increase in the amplitudes of the SST variations during the summer when the SST horizontal gradients are the largest. In addition, only to a limited extent are some clear propagation patterns observed.

In band 1 (Fig. 6) near mid-basin (21°W) some organized structures are evident beginning about JD 210 (late July). Phase speed, determined graphically from the

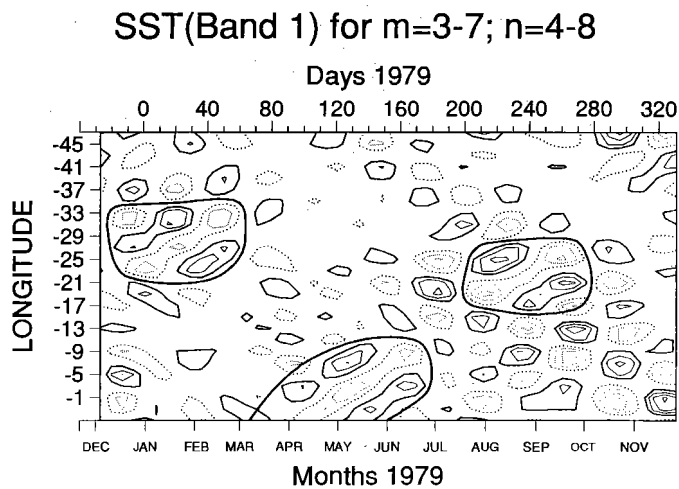


Figure 6

Band-1 (1924^{-1} - 825^{-1} cycles/km; 91^{-1} - 46^{-1} cycles/day) FGGE VOS SST field. Contour interval is 0.2 with 0°C contour suppressed. Number of dof=100. Dashed and solid contours denote negative and positive values respectively. Organized features are circled.

contour, is westward at about -20 cm/s but the structures are only organized from about JD 200 to JD 280 (July to October) in time and extend from about 25° to 13°W in space (a region of increased horizontal temperature gradients near the equator, Figs. 1 and 5). The wavelength and period are roughly 900-1100 km and 60-80 days respectively. Much earlier in the year

Table 2

Fractional variance in terms of AP filtered ($m=0-10$ space harmonics, or wave numbers to 577^{-1} cycles/km and $n=0-18$ time harmonics, or frequencies to 20^{-1} cycles/day) SST field variance [1.55 (°C)]².

	Harmonic number/ wave number	Harmonic number/ frequency	Fractional variance w. r. t. AP	SST(*) variance
LP	0-3/ (1924^{-1} cycles/km)	0-4/ (91^{-1} cycles/day)	.70	—
Band I	3-7/ (1924^{-1} - 825^{-1} cycles/km)	4-8/ (91^{-1} - 46^{-1} cycles/day)	.042	0.65
Band W	»	10-17/ (37^{-1} - 21^{-1} cycles/day)	.063	.099
		Bands I; W Total :	[.106]	[.164]

(*) For bands I and W, variance= 0.164 (°C)². The two bands represent about 10% of the total AP variance.

some structures are apparent near 25°W in January and again near 5°W in May (JD 120). These features seem to persist for about a month. Phase speed is still about -20 cm/s.

In band W (Fig. 7), beginning in June (JD 160) and near 20°W-25°W, structures with apparent westward phase propagation advance eastward to near 1°-4°W by August (JD 220). Again, estimates of period wavelength and phase propagation speed can be determined directly from the plots. The dominant temporal and spatial scales are about 28 days and 1100 km respectively. The associated phase speed (westward) is about -50 cm/s and the whole pattern moves eastward at approximately 30 cm/s.

SST(Band W) for $m=3-7$; $n=10-17$

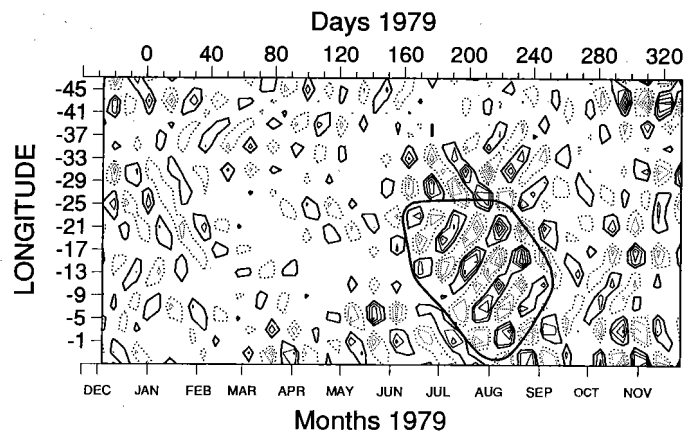


Figure 7

Band-W (1924^{-1} - 825^{-1} cycles/km; 37^{-1} - 21^{-1} cycles/day) FGGE VOS SST field. Contour interval is 0.2 with 0°C contour suppressed. Number of dof=160. Dashed and solid contours denote negative and positive values respectively. Instability features are circled.

The designation W for the second band is to emphasize its width. Eight time harmonics were used to construct the inverted field in Figure 7 (rather than five as used to construct band 1). Moreover, the pattern is relatively stable across this broad band of frequencies (37^{-1} - 21^{-1} cycles/day, Tab. 2). In particular, eliminating time harmonics 10-12, does not materially change the characteristics of the band's prominent features described above (the disturbance observed east of 25°W). Taken separately, the disturbance has a variance 2.5 times that of the background variance (variance of band W without the disturbance). At the 95% confidence level, the F test requires a variance ratio of

about 1.4 for $\text{dof} > 100$. It is likely therefore that the organized features in band W are significantly above background energy levels. These features of the variability in band W are similar to structures observed in the S/F data as described by Weisberg and Weingartner (1988). They appear to be related to waves that are generated by surface current instability after the springtime intensification of the surface winds. The SST variability that is thought to be related to the instability waves are shown in the band-pass filtered (6 db down at 37 days and 13 days) data of Figure 8a. A similar plot of the FGGE data is given in Figure 8b. Series were plotted at longitudes where disturbances were observed from Figure 7 (essentially at longitudes east of 25°W).

For completeness, the same analyses were performed on the SST field north and south of the equator, from 3° to 1°S, and also from 1° to 3°N. Tempered by the constraints of the quantity and quality of the FGGE VOS data set, there were few organized structures in either band 1 or band W either north or south of the equator. Interestingly enough, in the region where the instability-like features were observed on the equator east of 25°W beginning in June (Fig. 7) no prominent temperature structures are evident between 1° and 3°N. This contrasts with the study by Legeckis and Reverdin (1987) in which instability waves were observed in SST data derived from satellite observations during the early part of June 1983. They observed the largest north-south excursions of the SST front between 10° and 20°W with the mean position of the front near 1.4°N.

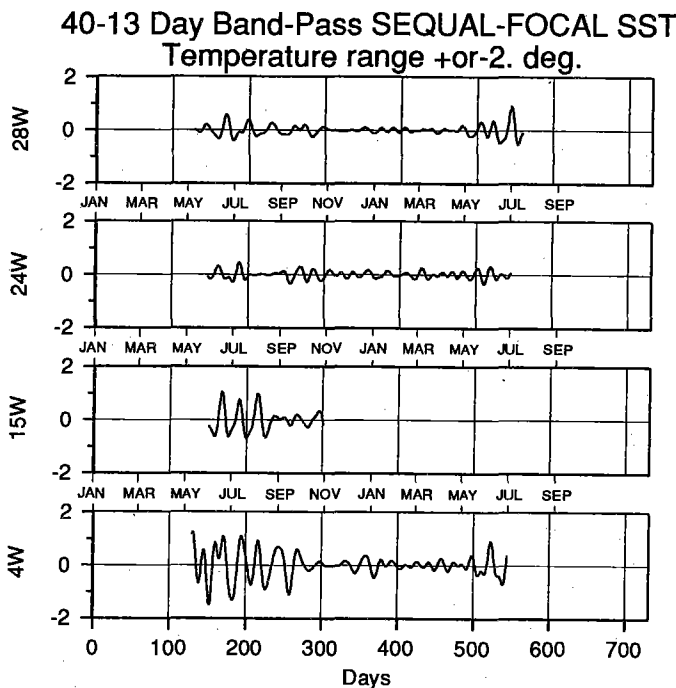


Figure 8a
(40-13)-day band-pass filtered S/F SST data during 1983-1984.

DISCUSSION

With regard to the easterly component of the surface wind stress field during 1979, except for a phase lag of

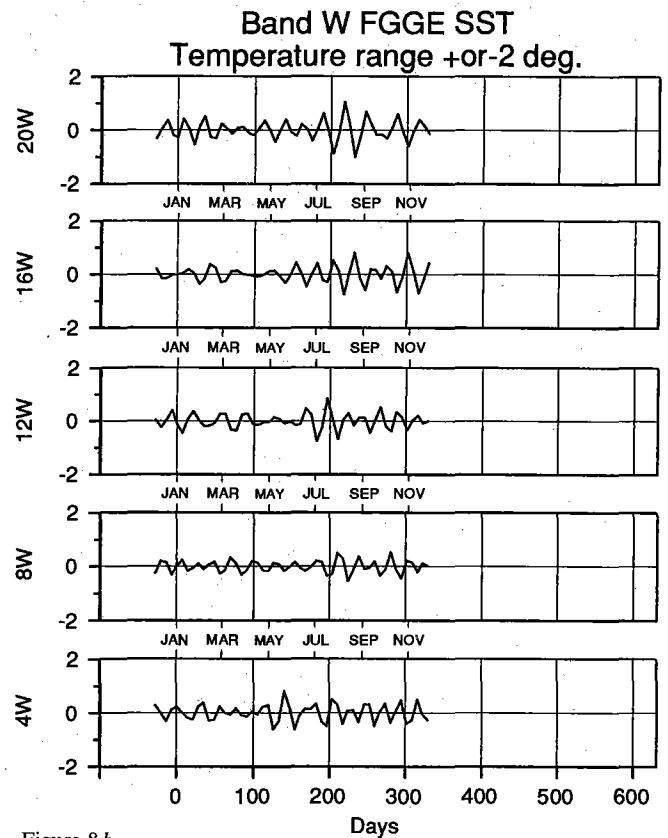


Figure 8b
Band-W ($37^{-1}-21^{-1}$ cycles/day) FGGE VOS SST times series for longitudes 20°, 16°, 12°, 8° and 4°W corresponding to longitudes where band-W SST disturbances are observed (Fig. 7). Zero days indicates January of 1979.

several weeks (Garzoli and Katz, 1984), the springtime transition from weak to strong easterlies was quite similar to that which occurred during the first year of the S/F experiment in 1983. Thus, we would expect to see some of the same SST structures observed by Weisberg and Weingartner (1988). They observed instability waves in the near-surface temperature and velocity data shortly after the springtime intensification (June) of the easterly wind stress in 1983. These waves were first observed by Duing *et al.* (1975) in the Atlantic Ocean and are attributed to barotropic instabilities (Philander, 1978). Weisberg and Weingartner (1988) determined that these instability waves are generated in the region of cyclonic shear right near the equator and that for the S/F data set, lasted for about three cycles, had a central periodicity and wavelength of about 25 days and (1100-1200) km respectively, and a westward phase speed of about -50 cm/s. The instabilities themselves moved eastward. These characteristics are consistent with the properties estimated from the band-W FGGE data in Figure 7 (phase speed of -50 cm/s; period and wavelength of 28 days and 1100 km respectively). Errors are no more than ± 5 cm/s from graphic scaling of the SST contours. These structures were detected in a fairly wide band (band W, Tab. 2) and are stable over a broad range of time harmonics ($n=10, 17, 37^{-1}-21^{-1}$ cycles/day). The data also show that the disturbance progresses eastward (Fig. 7).

Inconsistencies arise in that the band-W FGGE data do not show larger amplitudes eastward. Conspicuously absent are the large amplitudes near 16°W (an area of

reduced data in the VOS fields in Figure 1) that appear in the S/F (40-13)-day band-pass filtered data (near 15°W) in Figure 8a. In addition, the disturbance in the FGGE data progresses at least to 4°W. This appears to be the case as well in the S/F data near 4°W, although Weisberg and Weingartner (1988) state that the instability is not manifest there in the horizontal velocity field. In this region (4°W) on the equator in the Gulf of Guinea, Houghton and Colin (1987) suggest that SST manifestations of Rossby-gravity wave fluctuations are forced by the local meridional wind as it intensifies in contrast to SST variations associated with instability waves in the middle of the equatorial Atlantic Ocean.

Because SST disturbances similar to those analyzed by Weisberg and Weingartner (1988) were detected in the band-W FGGE data set and are fairly stable with a signal to noise ratio of 2.5 as discussed above, we have some confidence in the SST structures observed in this band (Fig. 7). With regard to the structures in band 1 (Fig. 6), Garzoli and Katz (1984) report low frequency (periods greater than one month) fluctuations in the wind field at St. Peter and St. Paul Rocks (near 30°W just north of the equator). It is possible that an equatorial wind divergence field with these frequencies might be partly responsible for the features observed in band 1.

In conclusion, two-dimensional Fourier transforms provide a useful technique for analyzing VOS SST data. Analysis of the 1979 FGGE data showed SST signatures very similar to those observed with moored instrumentation during the S/F programs in 1983 and 1984. There are some limitations in using the VOS data, however. The weekly resolution can cause aliasing problems. Furthermore, the sampling interval is near the limits of the sampling requirements necessary to adequately resolve features like the instability waves with periods of 3-4 weeks. VOS data do have the advantage of basinwide coverage that would not ordinarily be available with conventional moorings. The use of VOS data and the analysis techniques employed herein, in conjunction with other data from *in situ* moorings and satellite-derived infrared imagery, are therefore warranted in future studies and monitoring schemes.

Acknowledgements

Support for D. A. M. and R. L. M. was provided in part by a grant from NOAA and the Office of Climate and Atmospheric Research and support for R. H. W. was provided by the Oceanography Section of the National Science Foundation under Grant OCE-8841927.

APPENDIX

The details of the two-dimensional Fourier analysis are herein described. For the field $z(x, t)$, the two-dimensional transform is,

$$I_{nm} = \frac{1}{LT} \int_0^L \int_0^T z(x, t) e^{-i\omega_n t} e^{-ik_m x} dt dx$$

and the four-sided inverse transform is,

$$z(x, t) = \sum_{m=-K/2}^{K/2} \sum_{n=-N/2}^{N/2} I_{nm} e^{i\omega_n t} e^{ik_m x}$$

where the function $[z(x, t)]$ of space (x) and time (t) is retrieved by summing up to the Nyquist wave number and frequency whose harmonics are $K/2$; $N/2$ respectively. The complex coefficients I_{nm} in terms of the real equivalent coefficient are,

$$I_{nm} = \frac{1}{4} [(C_{nm} - F_{nm}) - i(E_{nm} + D_{nm})].$$

The inverse transform in terms of the real equivalent coefficients (C_{nm} , D_{nm} , E_{nm} , F_{nm}) is

$$\begin{aligned} z(x, t) = & C_{00}/4 \\ & + \frac{1}{2} \sum_{m=1}^{K/2} (C_{0m} \cos k_m x + D_{0m} \sin k_m x) \\ & + \frac{1}{2} \sum_{n=1}^{N/2} (C_{n0} \cos \omega_n t + E_{n0} \sin \omega_n t) \\ & + \sum_{m=1}^{K/2} \sum_{n=1}^{N/2} (C_{nm} \cos \omega_n t \cos k_m x \\ & + F_{nm} \sin \omega_n t \sin k_m x \\ & + E_{nm} \sin \omega_n t \cos k_m x + D_{nm} \cos \omega_n t \sin k_m x). \end{aligned}$$

The temporal and spatial realization as in Figures 6 and 7 of a selected wave number and frequency band is obtained by invoking one of the above inverse transforms over the selected range of wave number harmonics (m) and frequency harmonics (n). The fractional variance (contoured in Fig. 4) is defined as

$$E_f = \frac{1}{4} (C_{nm}^2 + D_{nm}^2 + E_{nm}^2 + F_{nm}^2) / \text{VAR}$$

where VAR is the two-dimensional areal variance.

$$\text{VAR} = \frac{1}{LT} \int_0^L \int_0^T (z(x, t) - C_{00}/4)^2 dt dx.$$

REFERENCES

- Düling W., P. Hisard, E. Katz, J. Meincke, L. Miller, K. V. Moroshkin, G. Philander, A. A. Ribnikov, K. Voigt and R. Weisberg (1975).** Meanders and long waves in the equatorial Atlantic. *Nature*, **257**, 280-284.
- Garzoli S. and E. J. Katz (1984).** Winds at St. Peter and St. Paul rocks during the first SEQUAL year. *Geophys. Res. Letts.*, **11**, 715-718.
- Houghton R. W. and C. Colin (1987).** Wind-driven meridional eddy heat flux in the Gulf of Guinea. *J. Geophys. Res.*, **92**, 10, 777-10, 786.
- Legeckis R. and G. Reverdin (1987).** Long waves in the equatorial Atlantic Ocean during 1983. *J. Geophys. Res.*, **92**, 2835-2842.
- Molinari R. L., J. F. Festa and E. Marmolejo (1985).** Evolution of sea-surface temperature and surface meteorological fields in the tropical Atlantic Ocean during FGGE, 1979. I. Description of surface fields and computation of surface energy fluxes. *Prog. Oceanogr.*, **14**, 401-420.
- Philander S. G. H. (1978).** Instabilities of zonal equatorial currents, 2. *J. Geophys. Res.*, **83**, 3679-3682.
- Reynolds R. W. (1983).** A comparison of sea-surface temperature anomalies. *J. Climate Appl. Met.*, **22**, 447-459.
- Weisberg R. H. and C. Colin (1986).** Equatorial Atlantic Ocean temperature and current variations during 1983 and 1984. *Nature*, **322**, 6076, 240-243.
- Weisberg R. H. and T. J. Weingartner (1988).** Instability waves in the equatorial Atlantic Ocean. *J. Phys. Oceanogr.*, **18**, 1641-1657.
-